JOURNAL OF CATALYSIS 126, 434–450 (1990)

Bimetallic Promotion of Alcohol Production in CO Hydrogenation and Olefin Hydroformylation on RhFe, PtFe, PdFe, and IrFe Cluster-Derived Catalysts

ATSUSHI FUKUOKA,* TAKUMA KIMURA,* NOBUHIRO KOSUGI,† HARUO KURODA,† YOSHITAKA MINAI,† YOICHI SAKAI,† TAKESHI TOMINAGA,† AND MASARU ICHIKAWA*,[1]

*Catalysis Research Center, Hokkaido University, Sapporo 060, Japan and †Department of Chemistry, Faculty of Science, The University of Tokyo, Hongo, Tokyo 113, Japan

Received June 23, 1989; revised March 9, 1990.

Iron-containing bimetallic catalysts were prepared from carbonyl clusters as precursors deposited on SiO_2. $FeRh_4$ and Fe_2Rh_4 cluster-derived catalysts showed high activity and selectivity for formation of ethanol and methanol in CO hydrogenation. Fe_3Pt_3, Fe_6Pd_6, and $FeIr_4$ cluster catalysts gave methanol in high selectivity, while Fe-rich Fe_4Pt and Fe_4Pd were not selective catalysts. The RhFe cluster catalysts showed improved activity in hydroformylation of olefins; C_4-alcohols were substantially obtained from $C_3H_6 + CO + H_2$. Mössbauer and EXAFS studies on the Fe_2Rh_4/SiO_2 catalyst show that highly dispersed RhFe bimetallic particles are located on the SiO_2 surface, where Fe atoms exist preferentially in the state of Fe^{3+} even after H_2 reduction. FTIR spectra of CO chemisorbed on Fe_2Rh_4/SiO_2 exhibit a low-frequency band possibly due to the C- and O-bonded CO on Rh–Fe^{3+} sites. Bimetallic promotion of alcohol production in CO hydrogenation and olefin hydroformylation is proposed to originate from the two-site interaction of Rh–Fe^{3+} (or Pt–Fe^{3+}, Pd–Fe^{3+}, Ir–Fe^{3+}) sites with CO to enhance migratory CO insertion.

INTRODUCTION

The use of metal clusters as catalyst precursors is an important aspect of homogeneous and heterogeneous catalysis (*1–8*). The chemical modification of solid surfaces by using clusters has been investigated recently for the sophisticated control of metal particle sizes as small as 10 Å and well-defined metal compositions. The bimetallic clusters offer prospects of synergistic effect for the two metal components in many useful catalytic reactions. Since Sinfelt revealed by using EXAFS that alloys were formed in the reforming catalysts such as Pt–Ir and Ru–Cu on SiO_2 or Al_2O_3 (*9*), bimetallic clusters grafted on solid surfaces have attracted much attention, because they may provide the advantage of obtaining highly dispersed bimetallic particles which are managed at the molecular level (*10–12*). It has been reported that the bimetallic cluster-derived catalysts are active in the reactions such as skeletal rearrangement of hydrocarbons (*13–16*), hydrogenation of carbon–carbon multiple bonds (*16, 17*), CO hydrogenation (*2, 14, 15, 18–23*), hydroformylation of olefins (*24, 25*), and reductive carbonylation of nitro compounds (*26*).

In CO hydrogenation on salt-derived Rh/SiO_2 catalysts, some additive metal ions such as Mn, Ti, Zr, and Fe promote the production of oxygenates including methanol, ethanol, and acetic acid (*27*). In particular, Fe promotion on the salt-derived Rh–Fe/SiO_2 (*28, 29*), Pd–Fe/SiO_2 (*30*), and Ir–Fe/SiO_2 (*31, 32*) catalysts is remarkable for enhancing alcohol production. EXAFS (*33*), Mössbauer (*34, 35*), XPS (*36*), and FTIR (*37*) studies of the Rh–Fe/SiO_2 cata-

[1] To whom correspondence should be addressed.

0021-9517/90 $3.00

lysts suggested that this promotion was associated with Rh–Fe sites formed on the SiO_2 support.

Accordingly, as tailored models for the promoted Rh, Pt, Pd, and Ir, we have prepared RhFe, PtFe, PdFe, and IrFe catalysts from bimetallic carbonyl clusters deposited on SiO_2 (*38–40*). CO hydrogenation reaction was conducted on the RhFe, PtFe, PdFe, and IrFe catalysts. Hydroformylation reactions of ethylene and propylene have been carried out as a diagnostic reaction for migratory CO insertion which is an elementary step in CO hydrogenation. The structural properties of the catalysts have been studied by means of Mössbauer, EXAFS, and FTIR spectroscopies. In this paper, it is demonstrated that the bimetallic sites derived from carbonyl clusters are highly active for migratory CO insertion, and they provide high activity and selectivity toward alcohols. The origin of Fe promotion is discussed in terms of the two-site interaction with CO.

EXPERIMENTAL

Catalysts Preparation

Synthesis of clusters and their deposition onto SiO_2 were performed under an atmosphere of purified nitrogen using standard Schlenk and needlestock techniques (*41*). Solvents were stored under N_2 after being refluxed with and distilled from appropriate drying agents (hexane, CaH_2; THF, $LiAlH_4$; CH_3CN, P_4O_{10} followed by K_2CO_3; acetone, 4 A molecular sieves). Davison no. 57 (10–20 mesh, surface area = 280 $m^2\ g^{-1}$) was used as a silica support for catalytic reactions. The SiO_2 was heated at 320°C under vacuum (10^{-2} Pa) for 2 h and stored under N_2. When clusters are not stable in solutions under N_2, all manipulations were carried out under CO. Carbonyl clusters used in this work, references for their synthesis, and solvents employed in deposition of the clusters are listed in Table 1.

In a typical run, [TMBA][$FeRh_5(CO)_{16}$] (42 mg) was dissolved in 10 ml of THF, and 4 g of SiO_2 was added to the solution under N_2. After 30 min of stirring, the sample was evaporated to dryness at room temperature. The solid was oxidized in O_2 flow (1×10^5 Pa, 60 ml min^{-1}) at 150°C for 2 h in a glass tubing, followed by the reduction in H_2 flow (1×10^5 Pa, 60 ml min^{-1}) at the programmed temperature from 20 to 400°C (1.7°C min^{-1}) and 400°C for 2 h. After cooling, the sample was subjected to N_2 flow (1×10^5 Pa, 60 ml min^{-1}) for 30 min at room temperature; then 2 g of the sample was transferred to a reactor under air and reduced again in H_2 flow (1×10^5 Pa, 60 ml min^{-1}) at 400°C for 1 h prior to flowing a reaction gas. The total metal loading of this catalyst was 0.5 wt%. We use the notation $M_xM'_y/SiO_2$; the abbreviation refers only to the metal composition of the precursor cluster $M_xM'_y(CO)_z$ deposited on SiO_2.

Salt-derived Rh, Rh–Fe, Pt, Pd, Pd–Fe, and Ir–Fe/SiO_2 catalysts were prepared under air by adding SiO_2 to ethanol solutions of metal chlorides: $RhCl_3 \cdot 3H_2O$, $RhCl_3 \cdot 3H_2O$ + $FeCl_3$, $H_2PtCl_6 \cdot 6H_2O$, $PdCl_2$, $PdCl_2$ + $FeCl_3$, and $IrCl_4 \cdot H_2O$ + $FeCl_3$, respectively. After 30 min of stirring, the sample was evaporated to dryness using a rotary evaporator. Subsequent H_2 reduction and transference to the reactor were done as above.

CO Hydrogenation Reactions

A CO hydrogenation reaction was conducted at 250°C with a continuous flow stainless steel reactor (inner diameter = 14 mm, 240-mm-long tubing), where 2.0 g of the catalyst (total metal loading 2 wt%) was charged. A gas mixture of CO and H_2 ($CO : H_2 = 1 : 2$ molar ratio, 4.9×10^5 Pa) was introduced into the reactor at a flow rate of 90 ml min^{-1} and a space velocity of 1000 h^{-1}. Oxygenated products such as CH_3OH, CH_3CHO, and C_2H_5OH were collected in a water trap (50 ml of H_2O) by bubbling the effluent gas through it. Products were analyzed by gas chromatography. CO, CO_2, and C_1–C_4 hydrocarbons were separated by using a Shimadzu GC-8AIT gas chromatograph with a thermal conductivity detector. A column of 4 mmϕ × 1 m of active carbon (60–80 mesh) was used for separation of CH_4, CO, and CO_2 at room temperature.

TABLE 1

Catalyst Preparation of $RhFe/SiO_2$ (0.5 wt% of Metal) and PtFe, PdFe, and $IrFe/SiO_2$

Precursor	Ref.	Weight	Solvent	SiO_2	Atmosphere	Metal wt%
$Rh_4(CO)_{12}$	*42*	36 mg	hexane (10 ml)	4 g	N_2	0.5
$[TMBA]_2[Fe_3(CO)_{11}]^a$	*43*	93 mg	THF (10 ml)	4 g	N_2	0.5
$[TMBA]_2[FeRh_5(CO)_{16}]$	*44*	42 mg	THF (10 ml)	4 g	N_2	0.5
$[NMe_4]_2[FeRh_4(CO)_{15}]$	*44*	26 mg	THF (7 ml)	2 g	CO	0.5
$[TMBA]_2[Fe_2Rh_4(CO)_{16}]$	*44*	25 mg	THF (7 ml)	2 g	N_2	0.5
$Fe_3Rh_2(CO)_{14}C$	*45*	23 mg	THF (7 ml)	2 g	N_2	0.5
$Rh_4(CO)_{12}$ + $[TMBA]_2[Fe_3(CO)_{11}]$	—	32 + 11 mg	THF (10 ml)	4 g	N_2	0.5
$[NEt_4]_2[Pt_{12}(CO)_{24}]$	*46*	112 mg	THF (15 ml)	4 g	N_2	2
$[TMBA]_2[Fe_3Pt_3(CO)_{15}]$	*47*	158 mg	CH_3CN (15 ml)	4 g	N_2	2
$[TMBA]_2[Fe_4Pt(CO)_{16}]$	*48*	241 mg	CH_3CN (15 ml)	4 g	N_2	2
$[TMBA]_3[Fe_6Pd_6(CO)_{24}H]$	*48*	85 mg	acetone (10 ml)	2 g	N_2	2
$[TMBA]_2[Fe_4Pd(CO)_{16}]$	*48*	257 mg	CH_3CN (15 ml)	4 g	N_2	2
$[TMBA][HIr_4(CO)_{11}]$	*49*	67 mg	THF (10 ml)	2 g	CO	2
$[TMBA]_2[FeIr_4(CO)_{15}]$	*50*	75 mg	THF (10 ml)	2 g	CO	2

[a] TMBA = NMe_3Bz.

C_2–C_4 hydrocarbons such as ethylene and propylene were separated on a column of 4 mmϕ × 4 m *N,N*-dimethylformamide/Al_2O_3 (DMF 38%, 60–80 mesh) at room temperature. The concentration of the gaseous products in the off-gas was calibrated with the external standard method using a 5-ml sampler of gas. The analysis of the oxygenates dissolved in the water trap were performed on a Shimadzu GC-8APF gas chromatograph with a flame ionization detector using a 4 mmϕ × 4 m Chromosorb 101 (60–80 mesh) column at 135°C, and acetone was added as an internal standard. In each gas chromatography, concentrations of the products were calculated with an integrator (Shimadzu Chromatopac CR-3A).

Hydroformylations of Ethylene and Propylene

Hydroformylations of ethylene and propylene were carried out in vapor phase at atmospheric pressure with a flow-mode Pyrex glass reactor (i.d. = 14 mm, 240-mm-long tubing), where 2.0 g of the catalyst was charged. The metal loadings of the catalysts were 0.5 wt% for $RhFe/SiO_2$ and 2 wt% for PtFe, PdFe, and $IrFe/SiO_2$. Gas mixtures of C_2H_4 (or C_3H_6), CO, and H_2 (1 : 1 : 1 molar ratio, total pressure 1×10^5 Pa) were introduced into the reactor at a flow rate of 60 ml min^{-1} and a space velocity of 670 h^{-1}. The oxygenated products such as aldehydes and alcohols were collected by bubbling the effluent gas through a water trap (50 ml). C_2H_4 and C_2H_6 were separated by using the TCD–GC on a 4 mmϕ × 4 m Porapak Q (60–80 mesh) column at 70°C. C_3H_6 and C_3H_8 were separated on the 4 mmϕ × 4 m DMF/Al_2O_3 column at room temperature. The analysis of the oxygenated products dissolved in the water trap was conducted by the FID–GC. Propanal and 1-propanol were separated on the 4 mmϕ × 4 m Chromosorb 101 column at 150°C. Butanal, 2-methylpropanal, 1-butanol, and 2-methyl-1-propanol were separated on the same column at 155°C. Ethanol was added as an internal standard and an integrator was used for calculation of the concentrations of products.

Catalyst Characterization by ^{57}Fe Mössbauer, EXAFS, and FTIR Spectroscopies

Aerosil 300 (surface area = 300 ± 30 m^2 g^{-1}, average particle size = 7 mμ) was used

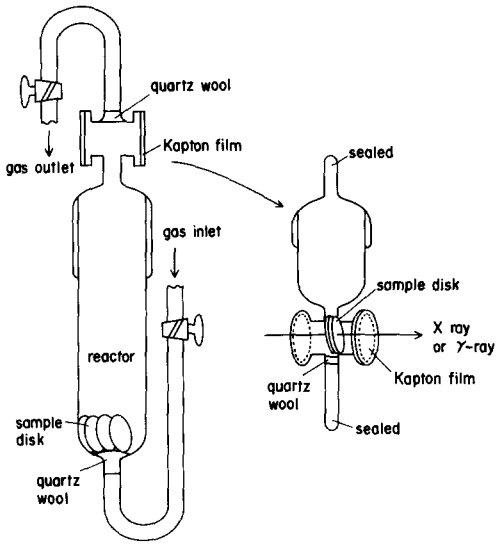

FIG. 1. An apparatus for H_2 reduction of sample disks (a) and a sealed cell for *in situ* EXAFS and Mössbauer (b).

as a silica support to prepare disks for spectroscopic studies, and the SiO_2 was treated *in vacuo* at 320°C for 2 h. Carbonyl clusters were deposited onto the SiO_2 under N_2, the sample was dried and oxidized by the same method described as above, and the sample was pressed into disks (20–40 mg, 20 mmϕ) under air. In Mössbauer and EXAFS study, the disks were reduced in an apparatus (Fig. 1) by flowing H_2 (50–100 ml min^{-1}) at the programmed temperature from 20 to 400°C (1.7°C min^{-1}) and 400°C for 2 h. Then the atmosphere in the cells was substituted for dry N_2 at room temperature. The sample disks were transferred to an *in situ* cell in the upper part; the lower part was attached to a glass-joint under N_2, and the cell was sealed. In FTIR study the sample disk was mounted into an *in situ* IR cell, and was reduced in H_2 flow using the same temperature program as above. After H_2 reduction, the atmosphere in the cell was evacuated. The total metal loading of the sample in each spectroscopy was 4 wt%.

Mössbauer spectra were obtained from the disks in the *in situ* cell (Fig. 1) with Kapton film windows on a Shimadzu MEG-2 or an Austin Science S-600 spectrometer at 20°C. In order to determine Mössbauer parameters and relative absorption areas, the spectra were fitted by computer as linear combination of Lorentzians with the least-squares method. Isomer shifts are given relative to α-Fe.

EXAFS spectra were obtained at Beam Line 10B in the Photon Factory (2.5 GeV, 90–150 mA) of the National Laboratory for High Energy Physics (KEK–PF) with a Si(311) channel-cut monochromator. Each experiment was done in the transmission mode on the disks in the *in situ* cell (Fig. 1) at 25°C. Analysis of the EXAFS data was performed with Program EXAFS1 and EXAFS2 (*51*). The EXAFS spectrum was extracted using a cubic spline method and normalized to the edge height. After conversion of photon energy E into photoelectron wave vector $\mathbf{k}$, the $\mathbf{k}^3$-weighted EXAFS spectrum was Fourier-transformed to r space, and the inversely Fourier-filtered data were analyzed with a curve fitting method on the basis of the short-range single-electron single-scattering theory (*52*) as expressed by

$$\mathbf{k}^3\chi(\mathbf{k}) = \sum_i (\mathbf{k}^2 N_i / ri^2) Si(\mathbf{k}) Fi(\mathbf{k}) \exp(-2\sigma i^2 \mathbf{k}^2) \sin(2\mathbf{k}ri + \phi i(\mathbf{k})),$$

where Ni, ri, Si(**k**), Fi(**k**), σi, and ϕi(**k**) represent a coordination number, an interatomic distance, a reduction factor, a backscattering amplitude, a Debye–Waller factor, and a phase shift, respectively. Table 2 summarizes the results of curve fitting analysis for some standard Rh, Pd, and Fe compounds, where the theoretical backscattering amplitude $F(\mathbf{k})$ and phase shift $\phi(\mathbf{k})$ functions were used (*53*). Interatomic distances are in good agreement with those from crystallographic values. The theoretical functions were used for the analysis of Fe–Rh and Fe–Pd bonds in the cluster-derived catalysts. To analyze Rh–Rh, Pd–Pd, Fe–Fe, and Fe–O bonds in the catalysts, we used the empirical backscattering amplitude and phase shift functions directly obtained

TABLE 2

Curve-Fitting Analysis of EXAFS Data for Standard Rh, Pd, and Fe Compounds

Sample	Bond	EXAFS					X-ray crystallography		
		N^a	r(Å)^b	ΔE_0(eV)^c	σ^2(Å^2)^d	R^e	N	r(Å)	Ref.
Rh foil	Rh–Rh	5.4	2.68	−11.43	0.0035	0.059	12	2.690	*54*
Pd foil	Pd–Pd	3.6	2.73	−13.33	0.0038	0.065	12	2.751	*54*
Fe foil	Fe–Fe	1.7	2.40	−19.80	0.0017	0.004	8	2.482	*54*
	Fe–Fe	5.0	2.81	−7.48	0.0055	0.004	6	2.866	*54*
$[Fe(H_2O)_6]^{3+}$(aq.)	Fe^{3+}–O	2.3	2.01	15.74	0.0016	0.070	6	2.07	*55*

[a] Coordination number.
[b] Interatomic distance.
[c] Inner potential correction.
[d] σ: Debye-Waller factor.
[e] R factor.

from the data of Rh, Pd, and Fe foils and $[Fe(H_2O)_6]^{3+}$ (aq.), respectively, where the Debye–Waller factors of the standard compounds were fixed at $\sigma_0 = 0.06$. The empirical functions were used with the fixed inner potential correction $\Delta E_0 = 0$ in the analysis of Rh–Rh, Pd–Pd, Fe–Fe, and Fe–O.

Infrared spectra were obtained from the disk in the *in situ* IR cell with CaF_2 windows on a double-beam Fourier transform infrared spectrometer (Shimadzu FTIR-4100) at a resolution of 2 cm^{-1}. Generally, 25–50 interferograms were coadded to improve signal-to-noise ratios.

RESULTS AND DISCUSSION

CO Hydrogenation on RhFe, PtFe, PdFe, and IrFe Carbonyl Cluster-Derived Catalysts

The results of CO hydrogenation at 4.9×10^5 Pa are summarized in Table 3, where the specific rates of product formation are evaluated on mol × min^{-1} × $(mol_{Rh,Pt,Pd,Ir})^{-1}$. Catalytic reactions were performed for 60 h after the beginning of syngas flow. All the catalysts had initially higher rates for hydrocarbons and lower rates for oxygenates, but changed gradually to oxygenates-producing catalysts. In each case, the catalytic activity reached steady state after 10–15 h on stream and remained constant for subsequent 45–50 h. The rates in Table 3 were estimated at steady state.

Rh_4/SiO_2 prepared from $Rh_4(CO)_{12}$ converted the 0.5% of CO and produced methane in 97% selectivity. The selectivity toward oxygenates in products was 3%; acetaldehyde mainly was obtained and a trace of methanol was produced, but ethanol was not produced. Fe_3/SiO_2 prepared from an anion cluster $[TMBA]_2[Fe_3(CO)_{11}]$ had no catalytic activity under the conditions of 250°C and 4.9×10^5 Pa. On the RhFe bimetallic catalysts prepared from $[TMBA]_2[Fe_2Rh_4(CO)_{16}]$ and $[NMe_4]_2[FeRh_4(CO)_{15}]$, the CO conversion and the rates for oxygenates were substantially increased. Notably, the rate for ethanol was strikingly enhanced on Fe_2Rh_4/SiO_2 and the selectivity toward ethanol reached to 33%. The RhFe catalysts improved the rates for methane as well, but relative enhancement of rates for oxygenates was much higher than that for methane. Accordingly, the selectivities toward methane were decreased to 79 and 56% on $FeRh_4/SiO_2$ and Fe_2Rh_4/SiO_2, respectively, which was in contrast with the substantial increase of the selectivities toward oxygenates such as methanol and ethanol. A salt-derived $Rh–Fe/SiO_2$ catalyst was prepared from $RhCl_3 \cdot 3H_2O$ and $FeCl_3$. The $Rh–Fe/SiO_2$ catalyst showed higher rates and selectivity to-

TABLE 3

CO Hydrogenation on SiO_2-Supported RhFe, PtFe, PdFe, and IrFe Carbonyl Cluster-Derived Catalysts[a]

Precursor/SiO_2	At ratio Fe/M	CO conv. (%)	Specific rate of formation[b] × 10^{-3} min^{-1}						Selectivity (%)[c]					
			CH_3OH	CH_3CHO	C_2H_5OH[d]	CH_4	CO_2	C_{2+}	CH_3OH	CH_3CHO	C_2H_5OH[d]	CH_4	CO_2	C_{2+}
$RhCl_3 \cdot 3H_2O$	0	0.1	0.03	0.18	0	36	0	0	<1	1	0	99	0	0
$Rh_4(CO)_{12}$	0	0.1	0.05	0.18	0	12	0	0	<1	3	0	97	0	0
$[NMe_4]_2[FeRh_4(CO)_{15}]$	0.25	1.5	3.7	1.4	1.7	39	0	0	8	6	7	79	0	0
$[TMBA]_2[Fe_2Rh_4(CO)_{16}]$[e]	0.50	2.4	7.0	1.3	13	45	0	0	9	3	33	56	0	0
$[TMBA]_2[Fe_3(CO)_{11}]$	—	0	—	—	—	—	—	—	—	—	—	—	—	—
$H_2PtCl_6 \cdot 6H_2O$	0	0.03	1.5	0	0	0	0	0	100	0	0	0	0	0
$[NEt_4]_2[Pt_{12}(CO)_{24}]$	0	0.1	4.2	0	0	0	0	0	100	0	0	0	0	0
$[TMBA]_2[Fe_3Pt_3(CO)_{15}]$	1.0	0.2	13	0	0	0	0	0	100	0	0	0	0	0
$[TMBA]_2[Fe_4Pt(CO)_{15}]$	4.0	1.7	12	0	0	31	88	23	7	0	0	18	50	26
$PdCl_2$	0	0.03	1.5	0	0	0	0	0	100	0	0	0	0	0
$[TMBA]_3[Fe_6Pd_6(CO)_{24}H]$	1.0	0.5	20	0	0	5	0	0	79	0	0	21	0	0
$PdCl_2 + FeCl_3$	1.0	0.5	5.4	0	0.2	11	9.2	4.8	17	0	1	34	28	20
$[TMBA]_2[Fe_4Pd(CO)_{16}]$	4.0	1.1	12	0	0	36	21	16	12	0	0	35	21	32
$[TMBA][HIr_4(CO)_{11}]$	0	0.01	0.2	0	0	0.3	0	<0.1	40	0	0	48	0	12
$[TMBA]_2[FeIr_4(CO)_{15}]$	0.25	0.66	45	0	0	4.3	0	0.4	90	0	0	9	0	1
$IrCl_4 \cdot H_2O + FeCl_3$	0.25	0.17	7.8	0	0.4	3.4	0	0.6	61	0	6	27	0	6
$[TMBA][HIr_4(CO)_{11}]$ + $[TMBA]_2[Fe_3(CO)_{11}]$	0.25	0.05	3.0	0	<0.1	0.8	0	0.1	79	0	0	20	0	2

[a] Reaction conditions: catalyst 2 g, total metal loading 2 wt%, reaction temperature 250 + 2°C, CO/H_2 = 0.5 molar ratio, total pressure 4.9 × 10^5 Pa, space velocity 1000 h^{-1}.

[b] mmol · $(mmol_{Rh,Pt,Pd,Ir})^{-1}$ · min^{-1}.

[c] Selectivities were calculated from the carbon efficiency: 100 × $iC/CO_{converted}$, i = carbon number of the product molecule, C = molar concentration of the product molecule.

[d] Including $CH_3COOC_2H_5$.

[e] TMBA = NMe_3Bz.

TABLE 4

Hydroformylation of Ethylene on SiO_2-Supported Rh, RhFe, and Fe Carbonyl Cluster-Derived Catalysts[a]

Precursor/SiO_2	At ratio Fe/Rh	C_2H_4 conv. (%)	Specific rate of formation,[b] min^{-1}		Selectivity, mol%	
			C_2H_6	EtCHO + 1-PrOH	Oxygenates[c]	Alcohol[d]
$Rh_4(CO)_{12}$	0	<0.1	0.006 (1)	0.002 (1)	28	0
[TMBA][$FeRh_5(CO)_{16}$][e]	0.20	3	0.16 (30)	0.13 (62)	45	4
[NMe_4]$_2$[$FeRh_4(CO)_{15}$]	0.25	5	0.28 (53)	0.20 (96)	42	2
[TMBA]$_2$[$Fe_2Rh_4(CO)_{16}$]	0.5	5	0.30 (57)	0.18 (86)	37	3
$Fe_3Rh_2(CO)_{14}C$	1.5	3	0.22 (41)	0.22 (110)	50	6
[TMBA]$_2$[$Fe_3(CO)_{11}$]	—	0	0	0	—	—
$Rh_4(CO)_{12}$ + [TMBA]$_2$[$Fe_3(CO)_{11}$]	0.26	0.7	0.039 (7)	0.036 (17)	48	0
$Rh_4(CO)_{12}/SiO_2$ + [TMBA]$_2$[$Fe_3(CO)_{11}$]/SiO_2	0.24	<0.1	0.003 (0.6)	0.001 (0.6)	27	0
[TMBA]$_2$[$Fe_2Rh_4(CO)_{16}$][f]	0.5	7	0.046	0.14	75	28

[a] Reaction conditions: catalyst 2 g, total metal loading 0.5 wt%, reaction temperature 135 ± 2°C, flow rate C_2H_4 + CO + H_2 = 20 + 20 + 20 ml min^{-1}, total pressure 1 × 10^5 Pa, space velocity 670 h^{-1}. Values in parentheses are rates relative to $Rh_4(CO)_{12}$.

[b] mmol · $(mmol_{Rh})^{-1}$ · min^{-1}.

[c] (EtCHO + 1-PrOH)/(C_2H_6 + EtCHO + 1-PrOH) × 100.

[d] 1-PrOH/(EtCHO + 1-PrOH) × 100.

[e] TMBA = NMe_3Bz

[f] Catalyst 2 g, total metal loading 2 wt%, total pressure 4.9 × 10^5 Pa, flow rate C_2H_4 + CO + H_2 = 20 + 20 + 20 ml min^{-1}.

ward oxygenates than Fe-free Rh_4/SiO_2, but the selectivity toward ethanol was lower than that on Fe_2Rh_4/SiO_2 at the same Fe/Rh ratio of 0.5.

Remarkable Fe-promotion for methanol was observed on PtFe, PdFe, and IrFe cluster-derived catalysts. Pt_{12}/SiO_2 prepared from [NEt_4][$Pt_{12}(CO)_{24}$] produced only methanol, and the rate for methanol was larger than that on a $H_2PtCl_6 \cdot 6H_2O$-derived catalyst. Fe_3Pt_3/SiO_2 (Fe/Pt = 1 atomic ratio) prepared from [TMBA]$_2$[$Fe_3Pt_3(CO)_{15}$] gave higher activity for methanol with the selectivity of 100%. Interestingly, hydrocarbons and CO_2 along with methanol were produced on the catalyst derived from Fe-rich [TMBA]$_2$ [$Fe_4Pt(CO)_{16}$] (Fe/Pt = 4); this poor selectivity may be due to the segregation of the bimetallic cluster making Fe metals active for hydrocarbons and CO_2, like the product distribution in Fischer–Tropsch synthesis. Also, high activity for methanol was achieved on the catalyst derived from [TMBA]$_3$[$Fe_6Pd_6(CO)_{24}H$] (Fe/Pd = 1), and the methanol selectivity was 79%, but the Pd–Fe/SiO_2 catalyst prepared from $PdCl_2$ + $FeCl_3$ (Fe/Pd = 1) gave lower selectivity toward methanol. On the other hand, Fe-rich Fe_4Pd/SiO_2 (Fe/Pd = 4) from [TMBA]$_2$[$Fe_4Pd(CO)_{16}$] provided the activity and poor selectivity similar to those on the Fe_4Pt/SiO_2 catalyst.

Iron is a very effective promoter for the production of methanol in the IrFe cluster-derived catalyst. The rate for methanol on $FeIr_4/SiO_2$ prepared from [TMBA]$_2$ [$FeIr_4(CO)_{15}$] was dramatically enhanced by a factor of over 200 times compared with Fe-free Ir_4/SiO_2. In addition, the selectivity toward methanol was as high as 90% but the selectivity toward methane was suppressed to 9% on $FeIr_4/SiO_2$. To determine the effect of proximity of Ir and Fe in the precursor compounds, two Ir–Fe catalysts were

TABLE 5

Hydroformylation of Propylene on SiO_2-Supported Rh, RhFe, and Fe Carbonyl Cluster-Derived Catalysts[a]

Precursor/SiO_2	At ratio Fe/Rh	C_3H_6 conv. (%)	Specific rate of formation,[b] min^{-1}		Selectivity, mol%		
			C_3H_8	*n,i*-PrCHO[c] + *n,i*-BuOH[d]	Oxygenates[e]	Alcohol[f]	*n*-Isomer[g]
$Rh_4(CO)_{12}$	0	<0.1	0.001	0.0003 (1)			
$Rh_4(CO)_{12}$[h]	0	0.7	0.027	0.0038	13	0	75
[TMBA][$FeRh_5(CO)_{16}$][i]	0.20	1	0.078	0.037 (13)	32	46	72
[NMe_4]$_2$[$FeRh_4(CO)_{15}$]	0.25	2	0.12	0.075 (260)	38	42	74
[TMBA]$_2$[$Fe_2Rh_4(CO)_{16}$]	0.50	2	0.13	0.088 (300)	41	44	73
$Fe_3Rh_2(CO)_{14}C$	1.5	1	0.10	0.084 (290)	45	63	70
[TMBA]$_2$[$Fe_3(CO)_{11}$]	—	0	0	0			
$Rh_4(CO)_{12}$ + [TMBA]$_2$[$Fe_3(CO)_{11}$]	0.26	0.2	0.015	0.010 (34)	41	33	78

[a] Reaction conditions: catalyst 2 g, total metal loading 0.5 wt%, reaction temperature 162 ± 2°C, flow rate C_3H_6 + CO + H_2 = 20 + 20 + 20 ml min^{-1}, total pressure 1 × 10^5 Pa, space velocity 670 h^{-1}. Values in parentheses are rates relative to $Rh_4(CO)_{12}$.

[b] mmol · $(mmol_{Rh})^{-1}$ · min^{-1}.

[c] *n*-PrCHO = butanal, *i*-PrCHO = 2-methylpropanal.

[d] *n*-BuOH = 1-butanol, *i*-BuOH = 2-methyl-1-propanol.

[e] (*n,i*-PrCHO + *n,i*-BuOH)/(C_3H_8 + *n,i*-PrCHO + *n,i*-BuOH) × 100.

[f] (*n,i*-BuOH)/(*n,i*-PrCHO + *n,i*-BuOH) × 100.

[g] (*n*-PrCHO + *n*-BuOH)/(*n,i*-PrCHO + *n,i*-BuOH) × 100.

[h] Catalyst 0.5 g, space velocity 1000 h^{-1}, total metal loading 4 wt%.

[i] TMBA = NMe_3Bz.

prepared from $IrCl_4 \cdot H_2O$ + $FeCl_3$ and a mixture of monometallic clusters [TMBA][$HIr_4(CO)_{11}$] and [TMBA]$_2$[$Fe_3(CO)_{11}$] at the same Fe/Ir atomic ratio of 0.25 as that of [TMBA]$_2$[$FeIr_4(CO)_{15}$]. Both catalysts gave larger rates for methanol than Ir_4/SiO_2, but the relative enhancement of rates was much lower than that with $FeIr_4/SiO_2$. On the salt-derived and the mixed monometallic cluster-derived catalysts, methanol selectivities were 60–80% and methane was substantially produced in above 20% of selectivity.

Hydroformylation of Ethylene and Propylene on RhFe, PtFe, PdFe, and IrFe Cluster-Derived Catalysts

Since CO hydrogenation over supported metal catalysts is composed of many elementary steps, it is difficult to discriminate between the influence of Fe on the individual elementary steps for alcohol production. Sachtler and Ichikawa (*27*) have suggested that alcohols are produced through surface acyls formed by the CO insertion into metal–alkyl bonds. Hydroformylation of olefins on Rh/SiO_2 enabled them to observe the specific influence of promoters on the migratory CO insertion and on the H addition to surface alkyl group. Accordingly, to unravel the promotive effect for production of methanol and ethanol from syngas on Fe-containing Rh, Pt, Pd, and Ir cluster catalysts, hydroformylations of ethylene and propylene were chosen as diagnostic reactions to evaluate the CO insertion.

Table 4 summarizes the results of hydroformylation of ethylene on SiO_2-supported RhFe cluster-derived catalysts. In all runs, the activity reached steady state after 5 h on stream and remained constant for subsequent 55 h. The rates were estimated at steady state. Under the conditions of 135°C

TABLE 6

Hydroformylation of Ethylene on SiO_2-Supported PtFe, PdFe, and IrFe Carbonyl Cluster-Derived Catalysts[a]

Precursor/SiO_2	At ratio Fe/M	C_2H_4 conv. (%)	Specific rate of formation,[b] min^{-1}		Selectivity, mol%	
			C_2H_6	EtCHO + 1-PrOH	Oxygenates[c]	Alcohol[d]
$[NEt_4][Pt_{12}(CO)_{24}]$	0	0.7	0.021	0.0056 (1)	2	8
$[TMBA]_2[Fe_3Pt_3(CO)_{15}]$[e]	1.0	0.8	0.021	0.019 (3.5)	48	37
$[TMBA]_2[Fe_4Pt(CO)_{16}]$	4.0	<0.1	0.003	0.0043 (0.8)	61	50
$PdCl_2$	0	9	0.20	0.0009 (1)	<1	≃0
$[TMBA]_3[Fe_6Pd_6(CO)_{24}H]$	1.0	55	1.8	0.035 (39)	2	79
$[TMBA]_2[Fe_4Pd(CO)_{16}]$	4.0	8	0.54	0.0041 (4.6)	1	91
$[TMBA][HIr_4(CO)_{11}]$[f]	0	0.3	0.0094	0.0003 (1)	3	70
$[TMBA]_2[FeIr_4(CO)_{15}]$[f]	0.25	0.4	0.012	0.0039 (13)	3	94

[a] Reaction conditions: catalyst 2 g, total metal loading 2 wt%, reaction temperature 135 ± 2°C, flow rate C_2H_4 + CO + H_2 = 20 + 20 + 20 ml min^{-1}, total pressure 1 × 10^5 Pa, space velocity 670 h^{-1}. Values in parentheses are rates relative to Fe-free catalysts.

[b] $mmol/mmol_{Pt,Pd,Ir}/min$.

[c] (EtCHO + 1-PrOH)/(C_2H_6 + EtCHO + 1-PrOH) × 100.

[d] 1-PrOH/(EtCHO + 1-PrOH) × 100.

[e] TMBA = NMe_3Bz.

[f] Reaction temperature 170°C.

TABLE 7

Hydroformylation of Propylene on SiO_2-Supported PtFe, and PdFe Carbonyl Cluster-Derived Catalysts[a]

Precursor/SiO_2	At ratio Fe/M	C_3H_6 conv. (%)	Specific rate of formation,[b] min^{-1}		Selectivity, mol%		
			C_3H_8	*n,i*-PrCHO[c] + *n,i*-BuOH[d]	Oxygenates[e]	Alcohol[f]	*n*-Isomer[g]
$[NEt_4]_2[Pt_{12}(CO)_{24}]$	0	0.1	0.0035	0.001 (1)	21	41	74
$[TMBA]_2[Fe_3Pt_3(CO)_{15}]$[h]	1.0	0.4	0.011	0.0074 (7.7)	40	97	60
$[TMBA]_2[Fe_4Pt(CO)_{16}]$	4.0	0.4	0.0014	0.0014 (1.5)	51	88	50
$[TMBA]_3[Fe_6Pd_6(CO)_{24}H]$	1.0	24	0.81	0.005	<1	98	41
$[TMBA]_2[Fe_4Pd(CO)_{16}]$	4.0	2	0.16	0.0007	<1	≃100	42

[a] Reaction conditions: catalyst 2 g, total metal loading 2 wt%, reaction temperature 162 ± 2°C, flow rate C_3H_6 + CO + H_2 = 20 + 20 + 20 ml min^{-1}, total pressure 1 × 10^5 Pa, space velocity 670 h^{-1}. Values in parentheses are rates relative to $[NEt_4]_2[Pt_{12}(CO)_{24}]$.

[b] mmol · $(mmol_{pt,Pd})^{-1}$ · min^{-1}.

[c] *n*-PrCHO = butanal, *i*-PrCHO = 2-methylpropanal.

[d] *n*-BuOH = 1-butanol, *i*-BuOH = 2-methyl-1-propanol.

[e] (*n,i*-PrCHO + *n,i*-BuOH)/(C_3H_8 + *n,i*-PrCHO + *n,i*-BuOH) × 100.

[f] (*n,i*-BuOH)/(*n,i*-PrCHO + *n,i*-BuOH) × 100

[g] (*n*-PrCHO + *n*-BuOH)/(*n,i*-PrCHO + *n,i*-BuOH) × 100.

[h] TMBA = NMe_3B_z

and 1 × 10^5 Pa, simple hydrogenation of ethylene to ethane is predominant over hydroformylation on Rh_4/SiO_2; the selectivity toward oxygenates, expressed by the percentage of (propanol + 1-propanol) to (ethane + propanal + 1-propanol), is only 28%. On Fe_3/SiO_2 derived from $[TMBA]_2[Fe_3(CO)_{11}]$, neither hydroformylation nor simple hydrogenation occurred under the reaction conditions.

The activity for hydroformylation was greatly increased on the catalysts derived from RhFe clusters with the metal composition of $FeRh_5$, $FeRh_4$, Fe_2Rh_4, and Fe_3Rh_2; the rates for EtCHO + 1-PrOH were improved by factors of 62–110 compared with Fe-free Rh_4/SiO_2. The RhFe catalysts improved the activity for the simple hydrogenation, but the relative enhancement of rates for the simple hydrogenation was lower than that for the hydroformylation. The selectivity toward oxygenates was thus substantially increased on the RhFe catalysts: 28% on the Rh_4/SiO_2, 37–50% on the $RhFe/SiO_2$. A small amount of 1-PrOH was obtained on the RhFe catalysts, although Rh_4/SiO_2 gave only EtCHO as an oxygenate. To clarify the effect of the proximity of Rh and Fe in the catalysts, a mixed Rh–Fe catalyst was prepared by impregnation of SiO_2 with a THF solution of $Rh_4(CO)_{12}$ and $[TMBA]_2[Fe_3(CO)_{11}]$ at an atomic ratio of Fe/Rh = 0.26. The $Rh_4 + Fe_3/SiO_2$ catalyst gave much lower activity for the hydroformylation of ethylene than that from $[NMe_4]_2[FeRh_4(CO)_{15}]$ (Fe/Rh = 0.25). In addition, the two catalysts Rh_4/SiO_2 and Fe_3/SiO_2 were mixed at the Fe/Rh atomic ratio of 0.24 and charged into the reactor. The resulting $Rh_4/SiO_2 + Fe_3/SiO_2$ catalyst showed the activity for hydroformylation and hydrogenation as low as that by Rh_4/SiO_2.

Hydroformylation of ethylene under high pressure (4.9 × 10^5 Pa) on Fe_2Rh_4/SiO_2 derived from $[TMBA]_2[Fe_2Rh_4(CO)_{16}]$ was conducted in a stainless steel reactor. Compared with the catalytic performance at 1 × 10^5 Pa, the simple hydrogenation of C_2H_4 to C_2H_6 was effectively suppressed and the selectivity toward oxygenates reached 75% with considerable formation of 1-PrOH (28% selectivity among oxygenates).

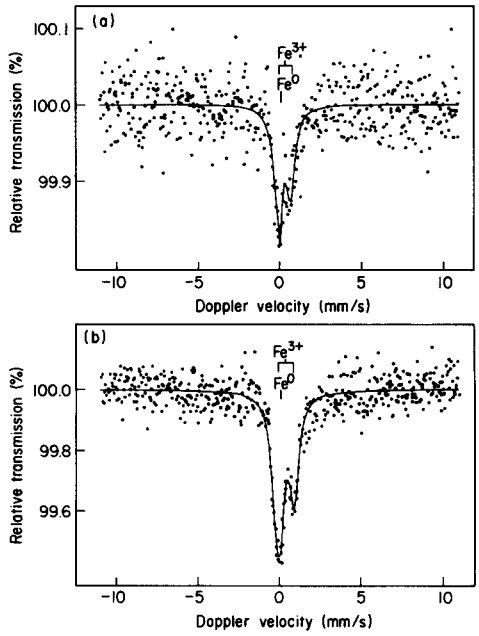

FIG. 2. ^{57}Fe Mössbauer spectra of H_2-reduced $FeRh_5/SiO_2$ (a) and Fe_2Rh_4/SiO_2 (b) catalysts at 20°C. H_2 reduction at 400°C for 2 h, isomer shifts relative to α-Fe.

Likewise, Fe promotion for the formation of oxygenates, in particular alcohols, was observed in hydroformylation of propylene, as shown in Table 5. At 162°C and 1 × 10^5 Pa, the rates of hydroformylation were dramatically increased on $FeRh_5$, $FeRh_4$, Fe_2Rh_4, and Fe_3Rh_2/SiO_2 catalysts, i.e., 130, 260, 300, and 290 times larger, respectively, relative to the $Rh_4(CO)_{12}$-derived catalyst. The selectivity toward hydroformylation was substantially increased on the RhFe catalysts; 13% on Rh_4/SiO_2, 32–45% on $RhFe/SiO_2$. Additionally, C_4-alcohols such as 1-butanol and 2-methyl-1-propanol were also obtained on the RhFe catalysts, while Rh_4/SiO_2 gave only aldehydes as oxygenates. Interestingly, the selectivity toward normal isomers of aldehydes and alcohols, i.e., (butanol + 1-butanol)/(butanal + 2-methylpropanal + 1-butanol + 2-methyl-1-propanol) × 100, was not affected by the Fe content

TABLE 8

Mössbauer Parameters of H_2-Reduced RhFe, PtFe, and PdFe Bimetallic Cluster-Derived Catalysts at 20°C[a]

Precursor/SiO_2	At ratio Fe/*M*	Iron state	δ[b] (mm s^{-1})	Δ[c] (mm s^{-1})	Peak area (%)
$[TMBA][FeRh_5(CO)_{16}]$[d]	0.2	Fe^0	0.15	—	12
		Fe^{3+}	0.37	0.82	88
$[TMBA]_2[Fe_2Rh_4(CO)_{16}]$	0.5	Fe^0	0.17	—	27
		Fe^{3+}	0.46	1.00	73
$[TMBA]_2[Fe_3Pt_3(CO)_{15}]$	1.0	Fe^0	−0.06	—	35
		Fe^{3+}	0.72	0.76	65
$[TMBA]_3[Fe_6Pd_6(CO)_{24}H]$	1.0	Fe^{2+}	1.24	2.50	36
		Fe^{3+}	0.35	0.43	64
$[TMBA]_2[Fe_4Pd(CO)_{16}]$	4.0	Fe^0	0.59	—	14
		Fe^{2+}	1.16	2.15	86

[a] Total metal loading 4 wt%, H_2 reduction at 400°C for 2 h.
[b] Isomer shift relative to α-Fe.
[c] Quadrupole splitting.
[d] TMBA = NMe_3Bz.

in precursor clusters. For example, the selectivity was 75% on Rh_4/SiO_2 and the RhFe cluster-derived catalysts gave the normal selectivities of 70–74%. This implies that the CO insertion into metal–C_3H_7 to form metal–COC_3H_7 occurs on Rh atoms, and Fe does not impose such a steric hindrance around Rh as is caused by PPh_3 in homogeneous hydroformylation with $HRh(CO)(PPh_3)_3$ (*56*).

From these results of hydroformylations of ethylene and propylene on the RhFe catalysts, it is suggested that RhFe clusters provide Rh–Fe sites where Rh and Fe atoms are in close proximity, and they are highly active for hydroformylation, i.e., CO insertion and successive hydrogenation to give alcohols.

Tables 6 and 7 present the results of hydroformylation of ethylene and propylene on PtFe, PdFe, and IrFe cluster-derived catalysts. In ethylene hydroformylation (Table 6), PtFe, PdFe, and IrFe catalysts exhibited substantial promotion for the rates of hydroformylation compared with Fe-free Pt, Pd, and Ir catalysts, although the rates were much smaller than those on $RhFe/SiO_2$ (Table 4). The rates for ethane on Pd-based catalysts were much higher than on Pt- or Ir-based ones by a factor of $10–10^2$. Thus Fe_6Pd_6/SiO_2 gave a modest rate for hydroformylation, but the hydrogenation of C_2H_4 to C_2H_6 was greatly predominant with a 55% of ethylene conversion at 135°C and 1×10^5 Pa. Likewise in RhFe-catalyzed hydroformylation, selectivity toward alcohol was increased on PtFe, PdFe, and $IrFe/SiO_2$ catalysts. Also, the improved selectivity toward alcohol was obtained in the hydroformylation of propylene on PtFe and PdFe catalysts. The selectivities toward *n*-isomer was 74% on Fe_3Pt_3/SiO_2 and 41% on Fe_6Pd_6/SiO_2, while the rates for hydroformylation were very small.

^{57}Fe Mössbauer Spectroscopy

The valence states of Fe in RhFe, PtFe, and PdFe cluster-derived catalysts were studied by ^{57}Fe Mössbauer spectroscopy. The spectra of $FeRh_5/SiO_2$ and Fe_2Rh_4/SiO_2 at 20°C are shown in Fig. 2 and the Mössbauer parameters are summarized in Table 8. The isomer shifts and quadrupole splittings for $FeRh_5/SiO_2$ and Fe_2Rh_4/SiO_2 are very similar to those for the salt-derived $Rh–Fe/SiO_2$ catalysts previously reported

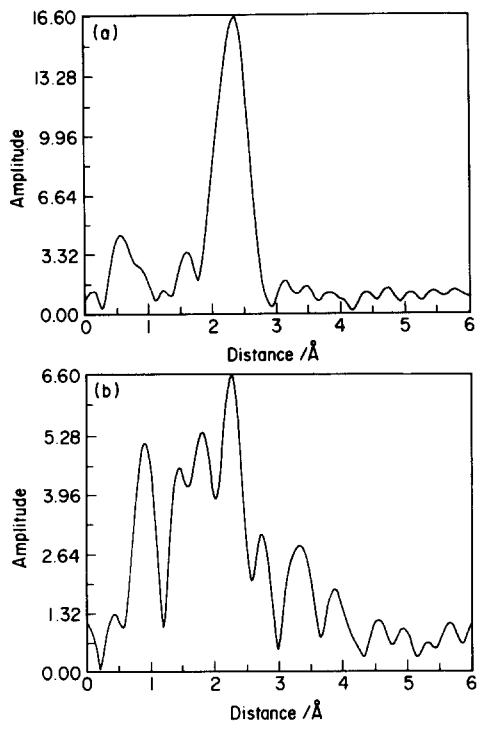

FIG. 3. Fourier Transforms of Rh K-edge EXAFS $\mathbf{k}^3$ χ (**k**) (a) and Fe K-edge EXAFS k^3 χ (k) (b) of Fe_2Rh_4/SiO_2 at 25°C after H_2 reduction at 400°C for 2 h.

(*35*). In Fig. 2, two absorption bands were observed and resolved into a singlet and a pair of quadrupole doublets by the computer fitting. The singlets at $\delta = 0.15$ mm s^{-1} were assigned to Fe^0 alloyed with Rh, but it is concluded that metallic iron was absent because the isomer shift was higher than that of α-Fe (0 mm s^{-1}). The isomer shifts and quadrupole splittings indicate that the doublets are to be attributed to Fe^{3+}. Niemantsverdriet *et al.* assigned the similar doublet in the salt-derived Rh–Fe/SiO_2 catalysts to high spin Fe^{3+} of iron(III) oxides with high dispersion (*34*). Bands of Fe^+ and Fe^{2+} were negligible for $FeRh_5/SiO_2$ and Fe_2Rh_4/SiO_2.

It is notable that Fe atoms of the RhFe catalysts mostly exist in the state of Fe^{3+} even after H_2 reduction at 400°C. The ratios of peak area of Fe^{3+}/Fe^0 were 88/12 for $FeRh_5/SiO_2$ (atomic ratio Fe/Rh = 0.2) and 73/27 for Fe_2Rh_4/SiO_2 (Fe/Rh = 0.5). The Fe^{3+}/Fe^0 ratio decreased with increasing the Fe/Rh atomic ratio of precursor clusters, implying that Fe^{3+} was reduced to Fe^0 on Rh in the Fe-rich bimetallic catalysts.

Similar proportions of Fe^{3+} and Fe^0 were obtained for Fe_3Pt_3/SiO_2 which was a selective catalyst for methanol in CO hydrogenation. The data for Fe_6Pd_6/SiO_2 show the presence of Fe^{3+} and Fe^{2+}, but the band associated with Fe^0 was not observed. On the other hand, Fe^{2+} had a large contribution in Fe_4Pd/SiO_2; the relative peak areas of Fe^{2+} and Fe^0 were 86 and 14%, respectively. The Fe^{3+} species, which was found in the selective alcohol catalysts such as Fe_2Rh_4/SiO_2 and Fe_3Pt_3/SiO_2, was not observed in the poorly selective Fe_4Pd/SiO_2.

EXAFS Spectroscopy

EXAFS analysis was performed on the ethanol selective Fe_2Rh_4/SiO_2 after H_2 reduction at 400°C. Fig. 3 shows the Fourier transforms of $\mathbf{k}^3$-weighted EXAFS oscillation $\mathbf{k}^3$ χ (**k**) at Fe K-edge and Rh K-edge. The results of the curve-fitting analysis are summarized with the previous results for salt-derived Rh–Fe/SiO_2 catalysts in Table 9. Since the EXAFS data of the cluster-derived catalysts were quite similar to those of the salt-derived catalysts, we could estimate the contribution around Rh or Fe in Fe_2Rh_4/SiO_2 according to the procedures of analysis for the salt-derived Rh–Fe catalysts (*33*).

In Fig. 3, the Fourier transform of $\mathbf{k}^3$ χ (**k**) for the Rh K-edge EXAFS shows a strong peak at about 2.3 Å. From the curve-fitting analysis of inverse Fourier transform of the peak, it is assigned to Rh-Rh: the interatomic distance (r) = 2.70 Å, the coordination number (N) = 5.6. The contribution of Rh–Fe interaction was not found in the curve fitting of Rh K-edge data. In the Fourier transform of $\mathbf{k}^3$ χ (**k**) for the Fe K-edge EXAFS of Fe_2Rh_4/SiO_2, a peak at ca. 2.2 Å is assigned to Fe–Rh from the curve-fitting analysis: r = 2.54 Å and N = 1.8. A shoulder peak at ca. 1.8 Å is Fe–O (r = 1.99 Å, N = 3.0), where O may be the surface

TABLE 9

Results of the Curve-Fitting Analysis of $\mathbf{k}^3\chi(\mathbf{k})$ of H_2-Reduced RhFe and PdFe Bimetallic Cluster-Derived Catalysts[a]

Precursor/SiO_2	Fe/Rh,Pd	Bond	N[b]	r(Å)[c]	ΔE_0(eV)[d]	$\Delta\sigma^2$(Å^2)[e]	R[f]
$[TMBA]_2[Fe_2Rh_4(CO)_{16}]$	0.5	Fe–O	3.0	1.99	[g]	0.0012	0.048
		Fe–Rh	1.8	2.54	−15.44	0.0052[h]	0.048
		Rh–Rh	5.6	2.70	[g]	0.0030	0.005
$RhCl_3 \cdot 3H_2O + FeCl_3$[i]	0.5	Fe–O	0.9	1.99	—	—	—
		Fe–Rh	4.0	2.62	—	—	—
		Rh–Rh	9.5	2.66	—	—	—
$[TMBA]_3[Fe_6Pd_6(CO)_{24}H]$	1.0	Fe–O	3.8	1.93	[g]	0.0005	0.003
		Fe–Fe	0.4	2.50	[g]	0.0012	0.012
		Fe–Pd	0.9	2.69	−6.07	0.0034[h]	0.012
		Pd–Pd	6.5	2.75	[g]	0.0008	0.042
$PdCl_2 + FeCl_3$[j]	0.45	Fe–Fe	0.9	2.46	—	—	—
		Fe–Pd	9.0	2.62	—	—	—
		Pd–Fe	4.6	2.63	—	—	—
		Pd–Pd	7.7	2.76	—	—	—

[a] Total metal loading 4 wt%, H_2 reduction at 400°C for 2 h. The EXAFS spectra were obtained at 25°C under N_2. The errors were estimated to be 0.03 Å for r and 0.4 for N.

[b] Coordination number.

[c] Interatomic distance.

[d] Inner potential corrections.

[e] $\sigma^2 - \sigma_0^2$: the difference of squares of Debye-Waller factors between samples and standard compounds.

[f] R factor.

[g] ΔE_0 is fixed at 0 eV when the empirical functions were used, see EXPERIMENTAL.

[h] σ^2.

[i] From Ref. (*33*).

[j] From Ref. (*58*).

oxygen of SiO_2. There is negligible contribution of Fe–Fe. In comparison to Rh–Fe/SiO_2 (Fe/Rh = 0.5) prepared from $RhCl_3 \cdot 3H_2O + FeCl_3$, the contribution of Rh–Rh is decreased but that of Fe–O is increased for Fe_2Rh_4/SiO_2, i.e., Rh–Rh: N = 5.6 for Fe_2Rh_4/SiO_2, 9.5 for the salt-derived Rh–Fe/SiO_2; Fe–O: N = 3.0 for Fe_2Rh_4/SiO_2, 0.9 for the salt-derived Rh–Fe/SiO_2. In addition, the total coordination numbers around Rh and Fe in Fe_2Rh_4/SiO_2 are about 6 and 5, respectively, which indicates that the average particle size is as small as 10 Å.

The image of $[TMBA]_2[Fe_2Rh_4(CO)_{16}]$ deposited on the silica surface of small particles of silicon was obtained by using high-resolution transmission electron microscopy (*57*). The shape of one molecule of cluster was hemispherical and its diameter was less than 10 Å at the metal loading of 2–4 wt%. Continued irradiation of electrons imposed the aggregation of two or three molecules during the observation. The particle size of the Rh–Fe/SiO_2 (Fe/Rh = 0.3) by TEM is reported to be 25 Å (*33*).

From the EXAFS and Mössbauer results for Fe_2Rh_4/SiO_2, we propose the following structural model. Most Fe atoms are in the 3+ state and located between Rh and O to form chemical bonds with the oxygen atoms of SiO_2. Since the contribution of Fe–Fe is negligible and the total coordination number around Fe is as low as 5, Fe atoms/ions are highly dispersed. Thus Fe^{3+} ions anchor Rh atoms onto the SiO_2 support to generate Rh–Fe^{3+}O bimetallic sites, and these Fe^{3+} ions

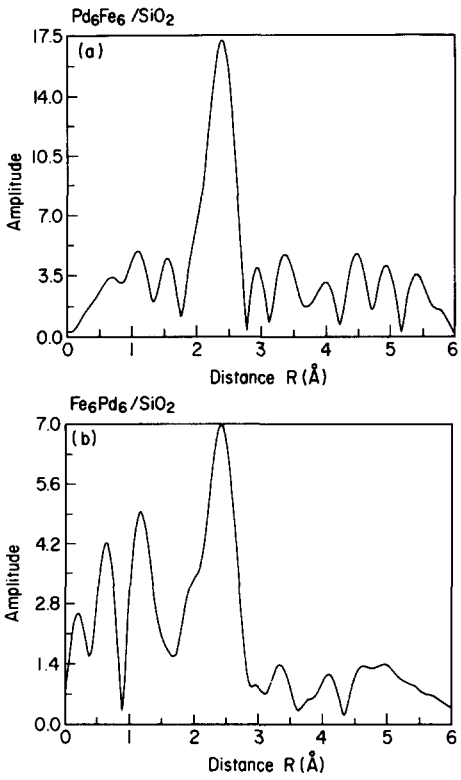

FIG. 4. Fourier Transforms of Pd K-edge EXAFS $\mathbf{k}^3$ χ (**k**) (a) and Fe K-edge EXAFS $\mathbf{k}^3$ χ (**k**) (b) of Fe_6Pd_6/SiO_2 at 25°C after H_2 reduction at 400°C for 2 h.

are stable and not reduced by H_2 at 400°C. Minor amounts of Fe are in the state of Fe^0, which may be located on the Rh surface to be subject to H_2-reduction in the presence of the noble metal Rh.

EXAFS study was performed on H_2-reduced Fe_5Pd_6 and Fe_4Pd/SiO_2 catalysts derived from bimetallic clusters. Fourier transforms of Pd and Fe K-edge EXAFS $\mathbf{k}^3$ χ (**k**) of Fe_6Pd_6/SiO_2 are shown in Fig. 4, and the results of the curve fitting analysis are summarized in Table 9. Two strong peaks were observed at 2.1–2.8 Å and 1.0–2.1 Å in the Fourier transform of EXAFS at the Fe K-edge. From the curve-fitting analysis, the former peak is assigned to the overlap of Fe–Fe (r = 2.50 Å, N = 0.4) and Fe–Pd (r = 2.62 Å, N = 0.9), and the latter to Fe–O (r = 1.93 Å, N = 3.8). The large contribution of Fe–O is consistent with the preferential existence of Fe^{3+} and Fe^{2+} in the Mössbauer results of Fe_6Pd_6/SiO_2. In the Fourier transform of EXAFS at the Pd K-edge, a strong peak was obtained at 1.9–2.8 Å, which was assigned to Pd–Pd (r = 2.75 Å, N = 6.5). The contribution of Pd–Fe and Pd–O was negligible. Although Fe–Pd was found in the Fe K-edge EXAFS, the contribution of Pd–Fe was not detectable in the Pd K-edge EXAFS.

By contrast, a large contribution of Fe–Fe and Fe–O was observed in the EXAFS results of Fe_4Pd/SiO_2, but Fe–Pd was negligible. The absence of Fe–Pd is reasonably reflected in the catalytic performance of the Fe_4Pd catalyst with a poor selectivity for the oxygenates in CO hydrogenation. In H_2-reduced Pd–Fe/SiO_2 catalysts prepared from $PdCl_2$ + $FeCl_3$, Fe–O bonding was not found and Fe atoms were proposed to be uniformly distributed in the metal particles

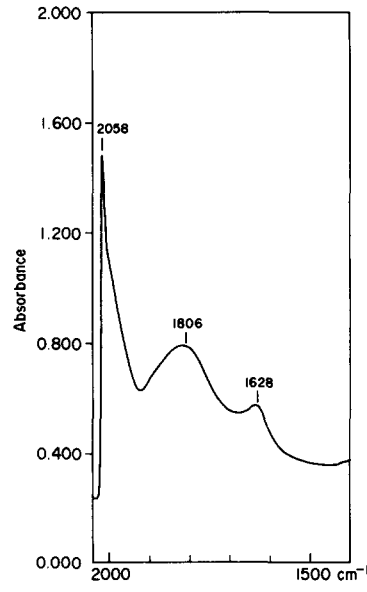

FIG. 5. FTIR spectrum of CO chemisorption on H_2-reduced Fe_2Rh_4/SiO_2. H_2 reduction at 400°C for 2 h, CO chemisorption at 25°C and 2.9 × 10^3 Pa for 30 min. The background spectrum was obtained on the disk which had been reduced with H_2 but not exposed to CO, and was substracted from the CO-chemisorbed spectrum.

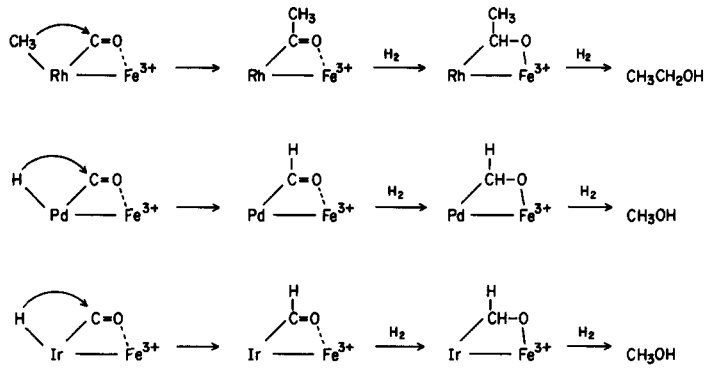

FIG. 6. Proposed mechanism for two-site activation of CO on M–Fe^{3+} (M = Rh, Pd, and Ir).

forming Pd–Fe^0 alloy (*58*). In contrast to this salt-derived catalyst, the results of Mössbauer and EXAFS on Fe_6Pd_6/SiO_2 imply that Fe ions are highly dispersed and located at the Pd–SiO_2 interface to anchor Pd atoms, where Pd–Fe^{3+} sites are generated on SiO_2 similarly as in the case of Fe_2Rh_4/SiO_2.

FTIR Spectroscopy

FTIR studies were performed on the CO chemisorption on Rh_4, $FeRh_5$, and Fe_2Rh_4/SiO_2 after H_2 reduction at 400°C. The spectrum for Fe_2Rh_4/SiO_2 is shown in Fig. 5. Two absorption bands at 2058 and 1806 cm^{-1} are assigned to terminal and bridging CO on Rh atoms. The relative intensities of the bridging CO to terminal CO in the spectra of $FeRh_5/SiO_2$ and Fe_2Rh_4/SiO_2 were suppressed compared to Fe-free Rh_4/SiO_2. This is possibly due to the isolation of Rh sites with Fe^0 and/or Fe^{3+}. Moreover, it is notable that a low-frequency band appeared at ca. 1630 cm^{-1} in the spectra of $FeRh_5/SiO_2$ and Fe_2Rh_4/SiO_2 (1628 cm^{-1} in Fig. 5). This may arise from η^2-CO with bonding of C–Rh and O–Fe^{3+} on Rh–Fe^{3+}/SiO_2. Such a low-frequency band was not observed for Rh_4/SiO_2. It was previously suggested that similar bifunctional chemisorption of CO occurred on salt-derived Rh–Mn, Rh–Ti, and Rh–Zr/SiO_2, where a large reduction of the CO frequency was induced (*37*). Shriver *et al.* (*59, 60*) demonstrate that the stoichiometric formation of adducts between metal carbonyls and Lewis acids arises from C- and O-bonded CO, and the rate of the methyl migration, i.e., CO insertion, to form the acetyl complex in $Mn(CH_3)(CO)_5$ is greatly increased by the adduct formation with $AlBr_3$, BF_3, and γ-Al_2O_3.

By combining the FTIR data with the structural model suggested by Mössbauer and EXAFS studies, it is conceivable that Fe-promotion for alcohol production could be explained in terms of the two-site activation of CO with Rh–Fe^{3+} to enhance the migratory CO insertion into Rh–H and Rh–alkyl, and to enhance the successive hydrogenation to alcohols (Fig. 6). Electropositive Fe^{3+} contiguous to Rh atoms are located at the interface of Rh and SiO_2 may play a role not only in anchoring Rh atoms without their aggregation but also in affecting catalytic performances to promote the oxygenate formation in CO hydrogenation and olefin hydroformylation. Similar two-site activation is suggested for the methanol production on Fe_3Pt_3, Fe_6Pd_6, and $FeIr_4$ cluster-derived catalysts.

CONCLUSION

We have revealed the benefits of bimetallic carbonyl clusters as precursors for the preparation of tailored RhFe, PtFe, PdFe, and IrFe catalysts. $RhFe/SiO_2$ catalysts derived from clusters gave high activity and selectivity toward oxygenates, particularly

toward ethanol in CO hydrogenation. Pt_3Fe_3, Pd_6Fe_6, and Ir_4Fe clusters provided the highly active catalysts for methanol from CO + H_2. The Fe-containing bimetallic catalysts effectively promote migratory CO insertion as judged by activity for olefin hydroformylation. This activity and selectivity may be due to the two-site interaction with C- and O-bonded CO on M–Fe^{3+} sites (M = Rh, Pt, Pd, and Ir), which appear to be generated from bimetallic clusters supported on SiO_2.

ACKNOWLEDGMENTS

This research was supported by the Iwatani Naoji Foundation and by a Grant-in-Aid for Scientific Research (62750774) from the Ministry of Education, Science, and Culture of Japan. We thank Dr. J. A. Hriljac and Dr. A. Fumagalli for synthesizing Fe_3Rh_2 and $FeIr_4$ carbonyl clusters, respectively, used in this study. EXAFS work has been performed under the approval of the Photon Factory Advisory Committee (Proposal No. 87-002 and 88-029).

REFERENCES

1. Muetterties, E. L., Rhodin, T. N., Band, E., Brucker, C. F., and Pretzer, W. R., *Chem. Rev.* **79,** 9 (1979).
2. Ichikawa, M., *CHEMTECH,* 674 (1982).
3. Ichikawa, M., *in* "Tailored Metal Catalysts" (Y. Iwasawa, Ed.), p.183. Reidel, Dordrecht, 1986.
4. Basset, J. M., and Ugo, R., *in* "Aspects of Homogeneous Catalysis" (R. Ugo, Ed.), Vol. 3, p. 127. Reidel, Dordrecht, 1977.
5. Yermakov, Y. I., Kuznetsov, B. N., and Zakharov, V. A., "Catalysis by Supported Complexes." Elsevier, Amsterdam, 1981.
6. Gates, B. C., Guczi, L., and Knözinger, H., Eds., "Metal Clusters in Catalysis." Elsevier, Amsterdam, 1986.
7. Basset, J. M., Gates, B. C., Candy, J. P., Choplin, A., Leconte, M., Quignard, F., and Santini, C., Eds., "Surface Organometallic Chemistry: Molecular Approaches to Surface Catalysis." Kluwer Academic Pub., Dordrecht, 1988.
8. Braunstein, P., and Rose, J., *in* "Stereochemistry of Organometallic and Inorganic Compounds" (I. Bernal, Ed.), Vol. 3, Elsevier, Amsterdam, 1988.
9. Sinfelt, J. H., *Acc. Chem. Res.* **10,** 15 (1977); **20,** 134 (1987).
10. Yokoyama, T., Yamazaki, K., Kosugi, N., Kuroda, H., Ichikawa, M., and Fukushima, T., *J. Chem. Soc., Chem. Commun.*, 962 (1984).
11. Ichikawa, M., *Polyhedron* **7,** 2351 (1988).
12. Choplin, A., Huang, L., Theolier, A., Gallezot, P., Basset, J. M., Siriwardane, U., Shore, S. G., and Mathieu, R., *J. Amer. Chem. Soc.* **108,** 4224 (1986).
13. Anderson, J. R., and Mainwaring, D. E., *J. Catal.* **35,** 162 (1974).
14. Shapley, J. R., Hardwick, S. J., Foose, D. S., Stucky, G. D., Churchill, M. R., Bueno, C., and Hutchinson, J. P., *J. Amer. Chem. Soc.* **103,** 7383 (1981).
15. Iwasawa, Y., and Yamada, M., *J. Chem. Soc., Chem. Commun.*, 675 (1985).
16. Castiglioni, M., Giodano, R., and Sappa, E., *J. Mol. Catal.* **40,** 65 (1987).
17. Scott, J. P., Budge, J. R., Rheingold, A. L., and Gates, B. C., *J. Amer. Chem. Soc.* **109,** 7736 (1987).
18. Guczi, L., Schay, Z., Lazar, K., Vizi, A., and Marko, L., *Surf. Sci.* **106,** 516 (1981).
19. Kuznetsov, V. L., Danilynk, A. F., Kolosova, I. E., and Yermakov, Y. I., *React. Kinet. Catal. Lett.* **21,** 249 (1982).
20. Ferkul, H. E., Stanton, D. J., McCowen, J. D., and Baird, M. C., *J. Chem. Soc., Chem. Commun.*, 955 (1982).
21. Choplin, A., Leconte, M., Basset, J. M., Shore, S. G., and Hsu, W.-L., *J. Mol. Catal.* **21,** 389 (1983).
22. Budge, J. R., Lucke, B. F., Gates, B. C., and Toran, J., *J. Catal.* **91,** 272 (1985).
23. Kaminsky, M., Yoon, K. J., Geoffroy, G. L., and Vannice, M. A., *J. Catal.* **91,** 338 (1985).
24. Ichikawa, M., *J. Catal.* **56,** 127 (1979); **59,** 67 (1979).
25. Fukuoka, A., Matsuzaka, H., Hidai, M., and Ichikawa, M., *Chem. Lett.*, 941 (1987).
26. Braunstein, P., Bender, R., and Kervennal, J., *Organometallics* **1,** 1236 (1982).
27. Sachtler, W. M. H., and Ichikawa, M., *J. Phys. Chem.* **90,** 4752 (1986).
28. Bhasin, M. M., Bartley, W. J., Ellgen, P. C., and Wilson, T. P., *J. Catal.* **54,** 120 (1978).
29. Fukushima, T., Arakawa, H., and Ichikawa, M., *J. Phys. Chem.* **89,** 4440 (1985).
30. Fukushima, T., Araki, K., and Ichikawa, M., *J. Chem. Soc., Chem. Commun.*, 148 (1986).
31. Fukushima, T., Ishii, Y., Onda, Y., and Ichikawa, M., *J. Chem. Soc., Chem. Commun.*, 1752 (1985).
32. Koningsberger, D. C., Borgmans, C. P. J. H., van Elderen, A. M. J., Kip, B. J., and Niemantsverdriet, J. W., *J. Chem. Soc., Chem. Commun.*, 892 (1987).
33. Ichikawa, M., Fukushima, T., Yokoyama, T., Kosugi, N., and Kuroda, H., *J. Phys. Chem.* **90,** 1222 (1986).
34. Niemantsverdriet, J. W., van der Kraan, A. M., and Delgass, W. N., *J. Catal.* **89,** 138 (1984).
35. Minai, Y., Fukushima, T., Ichikawa, M., and Tominaga, T., *J. Radioanal. Nucl. Chem.* **87,** 189 (1984).

36. Niemantsverdriet, J. W., van Kaam, J. A. C., Flipse, C. F. J., and van der Kraan, A. M., *J. Catal.* **96,** 58 (1985).
37. Ichikawa, M., and Fukushima, T., *J. Phys. Chem.* **89,** 1564 (1985).
38. Fukuoka, A., Ichikawa, M., Hriljac, J. A., and Shriver, D. F., *Inorg. Chem.* **26,** 3643 (1987).
39. Fukuoka, A., Kimura, T., and Ichikawa, M., *J. Chem. Soc., Chem. Commun.,* 428 (1988).
40. Kimura, T., Fukuoka, A., Fumagalli, A., and Ichikawa, M., *Catal. Lett.* **2,** 227 (1989).
41. Shriver, D. F., and Drezdzon, M. A., "The Manipulation of Air-Sensitive Compounds," 2nd ed. Wiley, New York, 1986.
42. Chini, P., and Martinengo, S., *Inorg. Chim. Acta* **3,** 315 (1969).
43. Hodali, H. A., and Shriver, D. F., *Inorg. Synth.* **20,** 222 (1980).
44. Ceriotti, A., Longoni, G., Pergola, R. D., Heaton, B. T., and Smith, D. O., *J. Chem. Soc. Dalton Trans.,* 1433 (1983).
45. Hriljac, J. A., Holt, E. M., and Shriver, D. F., *Inorg. Chem.* **26,** 2943 (1987).
46. Longoni, G., and Chini, P., *J. Amer. Chem. Soc.* **98,** 7225 (1976).
47. Longoni, G., Manassero, M., and Sansoni, M., *J. Amer. Chem. Soc.* **102,** 7973 (1980).
48. Longoni, G., Manassero, M., and Sansoni, M., *J. Amer. Chem. Soc.* **102,** 3242 (1980).
49. Malatesta, L., and Caglio, G., *J. Chem. Soc. Chem. Commun.,* 420 (1967).
50. Fumagalli, A., private communication.
51. Kosugi, N., and Kuroda, H., Program EXAFS1/V04 and EXAFS2/V03, Research Center for Spectrochemistry, Univ. Tokyo, Japan, 1987.
52. Teo, B. K., "EXAFS: Basic Principles and Data Analysis." Springer-Verlag, Berlin, 1986.
53. Teo, B. K., and Lee, P. A., *J. Amer. Chem. Soc.* **101,** 2815 (1979).
54. Weast, R. C., Ed., "CRC Handbook of Chemistry and Physics," 65th ed. CRC Press, Boca Raton, 1984.
55. Wells, A. F., "Structural Inorganic Chemistry," 5th ed. Clarendon Press, Oxford, 1984
56. Collman, J. P., Hegedus, L. S., Norton, J. R., and Finke, R. G., "Principles and Applications of Organotransition Metal Chemistry," 2nd Ed. University Science Books, Mill Valley, 1987.
57. Iijima, S., Moriyama, K., Fukuoka, A., and Ichikawa, M., unpublished results.
58. Kuroda, H., Yokoyama, T., Kosugi, N., Ichikawa, M., and Fukushima, T., *J. Phys.* **47,** C8-301 (1986).
59. Butts, S. B., Holt, E. M., Strauss, S. H., Alcock, N. W., Stimson, R. E., and Shriver, D. F., *J. Amer. Chem. Soc.* **101,** 5864 (1979).
60. Correa, F., Nakamura, R., Stimson, R. E., Burwell, Jr., R. L., and Shriver, D. F., *J. Amer. Chem. Soc.* **102,** 5112 (1980).